

A Phantom Bursting Mechanism for Episodic Bursting

Richard Bertram^{a,b,*}, Joseph Rhoads^a, Wendy P. Cimbora^a

^a*Department of Mathematics, Florida State University, Tallahassee, FL 32306-4510, USA*

^b*Programs in Neuroscience and Molecular Biophysics, Florida State University, Tallahassee, FL 32301, USA*

Received: 12 November 2007 / Accepted: 29 April 2008 / Published online: 22 July 2008
© Society for Mathematical Biology 2008

Abstract We describe a novel dynamic mechanism for episodic or compound bursting oscillations, in which bursts of electrical impulses are clustered together into episodes, separated by long silent phases. We demonstrate the mechanism for episodic bursting using a minimal mathematical model for “phantom bursting.” Depending on the location in parameter space, this model can produce fast, medium, or slow bursting, or in the present case, fast, slow, and episodic bursting. The episodic bursting is modestly robust to noise and to parameter variation, and the effect that noise has on the episodic bursting pattern is quite different from that of an alternate episodic burst mechanism in which the slow envelope is produced by metabolic oscillations. This mechanism could account for episodic bursting produced in endocrine cells or neurons, such as pancreatic islets or gonadotropin releasing neurons of the hypothalamus.

Keywords Bursting · Electrical oscillations · Pancreatic islets · Beta-cells · Endocrine cells · Neurons

1. Introduction

Electrical bursting, characterized by periods of electrical spiking followed by periods of rest, is a behavior often produced by electrically active cells. Examples include the R_{15} neuron of *Aplysia* (Alving, 1986), thalamic neurons (Crunelli et al., 1987), pyramidal neurons (Wong and Prince, 1981), trigeminal neurons (Del Negro et al., 1998), pancreatic β -cells (Dean and Mathews, 1970), and pituitary gonadotrophs (Stojilkovic et al., 1992). A more complex form of bursting, episodic or compound bursting, has been reported in pancreatic islets (Henquin et al., 1982; Zhang et al., 2003) and in gonadotropin releasing hormone (GnRH) neurons of the pituitary (Kuehl-Kovarik et al., 2002; Suter et al., 2000). This consists of episodes of several bursts, followed by long silent phases or “deserts.” While mathematical models of bursting are plentiful (Coombes and Bressloff, 2005), there

*Corresponding author.

E-mail address: Bertram@math.fsu.edu (Richard Bertram).

has been much less attention on episodic bursting. In this article, we describe one novel mechanism for episodic bursting, using a minimal model of an excitable cell.

In bursting models, the variables can typically be classified as either “fast” or “slow.” Analysis of bursting is facilitated by treating the slow variables as parameters and then examining the dynamics of the fast subsystem for a range of values of these parameters (fast/slow analysis). The bursting trajectory of the full system is then superimposed on the bifurcation diagram of the fast subsystem (Rinzel and Ermentrout, 1998). Many bursting models have a single slow variable, and the period of bursting is determined by the slow variable time constant (Chay and Keizer, 1983; Rinzel, 1985). Some models, however, have more than one slow variable, and the burst period is determined by some combination of the slow variable time constants (Bertram et al., 2000; Rinzel, 1987; Smolen et al., 1993).

We have previously developed a minimal model of bursting with two slow variables that is capable of generating burst periods of a very wide range, typical of what is observed in pancreatic β -cells (Bertram et al., 2000). This full range of burst periods can be obtained by varying a single parameter (g_{K1}), the conductance of an ionic current associated with the faster of the two slow variables. For large values of g_{K1} fast bursting is produced, driven entirely by the faster of the two slow variables (s_1). For small values of g_{K1} slow bursting is produced, driven by the slower of the two slow variables (s_2). For intermediate values of g_{K1} bursting patterns are produced with an intermediate period and driven by a combination of s_1 and s_2 .

In this article, we use the model of Bertram et al. (2000) to illustrate a mechanism through which episodic bursting can be produced. With this mechanism, the fast bursts that are part of a burst episode are driven by the faster s_1 variable. The slow oscillations that cluster bursts together with intervening deserts are driven by the slower variable s_2 . We use fast/slow analysis to analyze the episodic bursting pattern, and to understand how the episodic bursting is transformed into either fast or slow bursting with changes in the g_{K1} parameter. We then check robustness of the episodic bursting in two ways. First, we add different magnitudes of random channel noise to the system to determine which features of the episodic bursting pattern are most sensitive. This is important since neural systems are inherently noisy. Second, we explore the parameter space of two key parameters and classify the behaviors of the system at each point on the parameter grid.

The model used in the investigation is intentionally minimal so as to focus on the underlying mechanism of episodic bursting. This mechanism may apply to episodic bursting in excitable cells such as GnRH neurons, but more complex models incorporating ionic currents present in the cells would be required to fully understand cell-specific neuronal behaviors.

2. Mathematical model

The model we use was developed as a minimal model for bursting in pancreatic islets (Bertram et al., 2000). It was designed to be simple and generic; the important feature of the model is the way that the two slow variables interact with the fast subsystem. The identities of the various ionic currents and their specific functional forms are not important, and can be varied without losing the essential dynamics of the model. In this article, we investigate the behavior of the model in a region of parameter space that is

somewhat different from that in the original model. Otherwise, the two models are the same.

The planar fast subsystem is described by

$$\frac{dV}{dt} = -(I_{Ca} + I_{Kdr} + I_{leak} + I_{K1} + I_{K2})/C_m, \quad (1)$$

$$\frac{dn}{dt} = [n_\infty(V) - n]/\tau_n(V). \quad (2)$$

where V is the membrane potential and n is an activation variable (fraction of open channels) for the delayed rectifier current I_{Kdr} . The Ca^{2+} current I_{Ca} produces the upstroke of an impulse, while I_{Kdr} produces the downstroke. There is also a constant-conductance leakage current I_{leak} that helps the system reach the spike threshold. The two additional K^+ currents I_{K1} and I_{K2} have slowly changing conductances, and are responsible for packaging spikes into bursts or burst episodes. The membrane capacitance is given by the parameter C_m . Expressions for the ionic currents are:

$$I_{Ca} = g_{Ca}m_\infty(V)(V - V_{Ca}), \quad (3)$$

$$I_{Kdr} = g_{Kdr}n(V - V_K), \quad (4)$$

$$I_{leak} = g_{leak}(V - V_{leak}), \quad (5)$$

$$I_{K1} = g_{K1}s_1(V - V_K), \quad (6)$$

$$I_{K2} = g_{K2}s_2(V - V_K). \quad (7)$$

The parameters V_{Ca} , V_{leak} , and V_K are the Nernst potentials for the ionic currents. The parameters g_{Ca} , g_{Kdr} , g_{leak} , g_{K1} , and g_{K2} are the maximum conductances. The fraction of open channels of each current type, except for the constant-conductance leak, is represented by an activation variable. The Ca^{2+} current (which could be replaced by a Na^+ current in a neural model) activates very rapidly, so for simplicity activation is assumed to be instantaneous with steady state function $m_\infty(V)$. Other activation variables that change more slowly are described by differential equations. Equation (2) describes the rate of change of n , the activation variable for the I_{Kdr} current. This assumes first-order kinetics, with equilibrium function $n_\infty(V)$ and time scale function $\tau_n(V)$.

The other two activation variables, s_1 and s_2 , constitute the slow subsystem. They are also described by first-order kinetic equations:

$$\frac{ds_1}{dt} = [s_{1\infty}(V) - s_1]/\tau_{s_1}, \quad (8)$$

$$\frac{ds_2}{dt} = [s_{2\infty}(V) - s_2]/\tau_{s_2}. \quad (9)$$

The time constants for these variables are large, making s_1 and s_2 slow variables.

The equilibrium functions, $m_\infty(V)$, $n_\infty(V)$, $s_{1\infty}(V)$, and $s_{2\infty}(V)$ have the form of $x_\infty(V)$ below:

$$x_\infty(V) = \frac{1}{1 + e^{(vx-V)/sx}}. \quad (10)$$

Table 1 Parameter values used in the model

$g_{Ca} = 280$ pS	$g_{Kdr} = 1300$ pS	$g_{leak} = 25$ pS
$g_{K1} = 22$ pS	$g_{K2} = 16$ pS	$C_m = 4525$ fF
$V_{Ca} = 100$ mV	$V_K = -80$ mV	$V_{leak} = -40$ mV
$vm = -22$ mV	$sm = 7.5$ mV	$vn = -9$ mV
$sn = 10$ mV	$\bar{\tau}_n = 8.25$ ms	$vs_1 = -50$ mV
$ss_1 = 5$ mV	$vs_2 = -40$ mV	$ss_2 = 15$ mV
$\tau_{s1} = 1000$ ms	$\tau_{s2} = 30000$ ms	

The time scale function for n is:

$$\tau_n(V) = \frac{\bar{\tau}_n}{1 + e^{(V-vn)/sn}}. \quad (11)$$

Stochasticity is introduced in Fig. 7 by introducing a pool of stochastic leakage channels, rewriting I_{leak} as

$$I_{leak} = g_{leak}q(V - V_{leak}), \quad (12)$$

where $q = (1 + p)/2$ is the fraction of open channels. This scaling ensures that at least half of the leakage channels are open. As in de Vries and Sherman (2000), p satisfies the Langevin equation:

$$\frac{dp}{dt} = [\alpha_p(1 - p) + \beta_pp]/\tau_p + \sigma w. \quad (13)$$

The intensity of the noise, σ , decreases with the square root of the number of stochastic channels (Fox, 1997), N_{stoc} :

$$\sigma = [\alpha_p(1 - p) + \beta_pp]/[\tau_p N_{stoc}]^{1/2}. \quad (14)$$

The variable w is a Wiener process with mean 0 and variance Δt , where $\Delta t = 0.1$ ms is the numerical time step (Ermentrout, 2002). The parameters α_p and β_p reflect channel opening and closing rates, respectively, and they determine the equilibrium value of p in the absence of noise ($\sigma = 0$), $p_\infty = \alpha_p/(\alpha_p + \beta_p)$. The parameter τ_p is the time constant for the approach to equilibrium. We use $\alpha_p = 1$ and $\beta_p = 4$, so that $p_\infty = 0.2$ and $q_\infty = (1 + p_\infty)/2 = 0.6$. We then divide the original value of g_{leak} by q_∞ , so that the conductance of I_{leak} will be the same in the deterministic and stochastic simulations when $p = p_\infty$. Various values of N_{stoc} are used in Fig. 7.

Parameter values are listed in Table 1. Values different from those in the table are given in the figure captions. All simulations and bifurcation diagrams were calculated with the XPPAUT software package (Ermentrout, 2002). The CVODE numerical method was used to solve the deterministic differential equations. The stochastic forward Euler method was used to solve the stochastic differential equations. Because of differences in numerical error associated with the CVODE and Euler algorithms, there could be small differences in oscillation periods even in the absence of noise. All computer codes are available for free download at www.math.fsu.edu/~bertram/software/neuron.

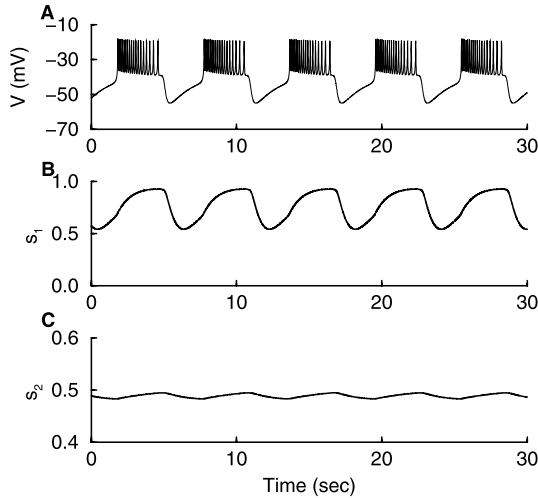


Fig. 1 (A) Fast bursting obtained with $g_{K1} = 20.5$ pS. (B) The activity-dependent rise and fall of the slow variable s_1 is primarily responsible for driving the bursting. (C) The slow variable s_2 is relatively constant during the fast bursting. However, the small oscillations in s_2 are essential for bursting in this example.

3. Fast bursting

The model produces fast bursting when the I_{K1} conductance is set at $g_{K1} = 20.5$ pS (Fig. 1). This bursting has a period of approximately 5 s and is driven primarily by s_1 , the faster of the two slow variables. This is evident in Figs. 1B, C, where significant oscillations in s_1 are clear, while s_2 is nearly constant. During the spiking or active phase of the burst s_1 increases. This increase activates the hyperpolarizing current I_{K1} , which accumulates throughout the active phase and eventually becomes large enough to terminate the burst. At this point, the membrane hyperpolarizes and as a consequence s_1 declines, but more slowly, deactivating I_{K1} . The deactivation of this current that occurs during the silent phase is responsible for initiating a new active phase of bursting. The s_2 variable behaves similarly to s_1 , but the amplitude of the oscillations is much smaller.

The bursting oscillation is best analyzed with a fast/slow analysis. Since s_2 undergoes only small oscillations about a mean value of $s_2 = 0.49$, we clamp s_2 at this value. The other slow variable is then treated as a bifurcation parameter for the fast subsystem (the V and n differential equations). This is illustrated in Fig. 2. For values of s_1 near 0 the fast subsystem has a steady state with a depolarized voltage $V \approx -20$ mV. As s_1 is increased the steady state goes through a supercritical Hopf bifurcation (HB) and loses stability (dashed curve). As s_1 is increased further a saddle node is reached (the upper knee, UK) and a middle branch of saddle points is formed. This middle branch ends at another saddle node (the lower knee, LK) and the steady state regains stability (the lower branch of the z -shaped curve). Emerging from the Hopf bifurcation is a branch of stable periodic solutions. These correspond to periodic spikes or action potentials. The periodic branch ends at a homoclinic bifurcation (HM) when it reaches the middle branch of the z -curve.

We now treat the s_1 - V plane as a phase plane, and superimpose the s_1 nullcline onto the bifurcation diagram. Finally, the bursting trajectory of the full system of equations is

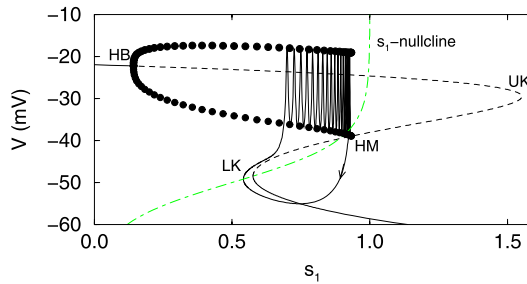


Fig. 2 Fast/slow analysis of fast bursting ($g_{K1} = 20.5$ pS and $s_2 = 0.49$ for the bifurcation diagram), see text for description. The solid portion of the z -curve represents branches of stable steady states. Dashed curves represent unstable steady states. The two branches of filled circles represent the maximum and minimum values of periodic solutions. The green dot-dashed curve is the s_1 nullcline. HB=supercritical Hopf bifurcation, HM=homoclinic bifurcation, LK=lower knee, UK=upper knee. (Color figure online.)

included. During the silent phase of bursting the trajectory moves to the left along the bottom branch of the z -curve since the trajectory is below the s_1 nullcline and $\frac{ds_1}{dt} < 0$. During the active phase, it moves to the right along the periodic branch since the trajectory is now above the nullcline. At the homoclinic bifurcation, the periodic branch ends and the trajectory returns to the stationary bottom branch.

As described, this is the standard scenario for square-wave or type 1 bursting (Bertram et al., 1995; Rinzel, 1987). However, the s_2 variable does actually play a role in this example of bursting. s_2 was clamped when the bifurcation diagram was constructed. However, with s_2 clamped the system does not burst. Depending on the clamping value, the V - n - s_1 subsystem is either silent (for larger s_2) or continuously spiking (for smaller s_2). Indeed, there are indications of this in Fig. 2. The s_1 nullcline intersects the stable stationary branch of the z -curve near the lower knee. This corresponds to a stable equilibrium of the full system. The nullcline also intersects the periodic branch of the z -curve near the homoclinic bifurcation. This could result in a stable periodic solution (continuous spiking) of the full system. (Because s_1 is only marginally slow, the full system trajectory could potentially escape from this intersection that is so close to the homoclinic bifurcation.) Thus, for bursting to be achieved with this system the s_2 variable must be allowed to vary. During the active phase s_2 increases marginally, shifting the z -curve to the left. This shift moves the homoclinic bifurcation leftward, past the s_1 -nullcline, allowing the phase point to move past the bifurcation and terminating the active phase. During the silent phase s_2 decreases marginally, shifting the z -curve to the right. This moves the lower knee to the right of the nullcline, allowing the phase point to move past the knee and terminating the silent phase. The effects of s_2 variation can also be seen in the s_1 time course, which has a fast rise followed by a slower rise during an active phase, rather than the monophasic rise that occurs in bursting models with a single slow variable.

4. Slow bursting

When the I_{K1} conductance is decreased to $g_{K1} = 20$ pS there is a dramatic change in the system dynamics. Rather than a fast bursting pattern, slow bursting is produced with

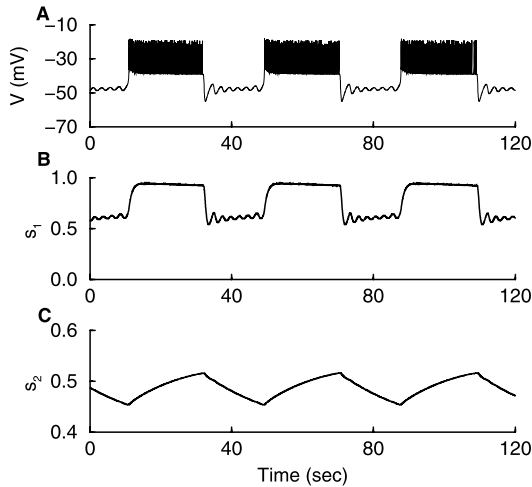


Fig. 3 (A) Slow bursting obtained with $g_{K1} = 20$ pS. (B) The s_1 variable now behaves more like a fast variable (on the time scale of bursting) than a slow variable, and exhibits subthreshold oscillations. (C) The s_2 variable now appears to be the primary driver of bursting.

small subthreshold oscillations during the silent phase (Fig. 3A). During the active phase s_1 rises and quickly saturates (Fig. 3B). The system remains in the active phase until s_2 rises sufficiently to turn off the spiking (Fig. 3C). During the silent phase, s_1 falls relatively rapidly and exhibits small oscillations, while s_2 declines more slowly and without oscillations. The decline in s_2 ultimately terminates the silent phase.

The slow bursting oscillation could be analyzed as before, in the $V-s_1$ plane. However, in this case, such an analysis does not reveal the mechanism for the subthreshold oscillations. An analysis in the $V-s_2$ plane is more revealing. Here, we treat s_1 as part of the fast subsystem, so this subsystem consists of the variables V , n , and s_1 , and s_2 is treated as the single slow variable. This is motivated by the observation that s_1 equilibrates early in the active and silent phases (Fig. 3), and so it has the characteristics of a fast variable.

Figure 4A shows the fast subsystem bifurcation diagram for this case. In order to focus in on the most important region of the diagram, the range of s_2 in the figure is restricted to the interval $[0.35, 0.55]$. The Hopf bifurcation that gives rise to the branch of stable periodic (spiking) solutions is not present in this interval, nor is the right knee. As before, the spiking branch terminates at a homoclinic bifurcation. However, the branch loses stability at a period doubling bifurcation (PD) long before it terminates. Importantly, a new Hopf bifurcation (HB) is present on the lower branch of the z -curve. This new bifurcation comes about via a codimension-2 Takens–Bogdanov bifurcation (Bertram et al., 1995). The new HB is a subcritical bifurcation that gives rise to a branch of unstable periodic solutions (open circles). This branch extends to the right and terminates at a homoclinic bifurcation. These unstable periodic solutions are small oscillations centered at the lower, hyperpolarized, steady state.

Superimposed on the bifurcation diagram in Fig. 4B are the s_2 nullcline and the burst trajectory of the full system of equations. During the active phase, the trajectory moves rightward along the periodic spiking branch. This branch loses stability at the PD bifurca-

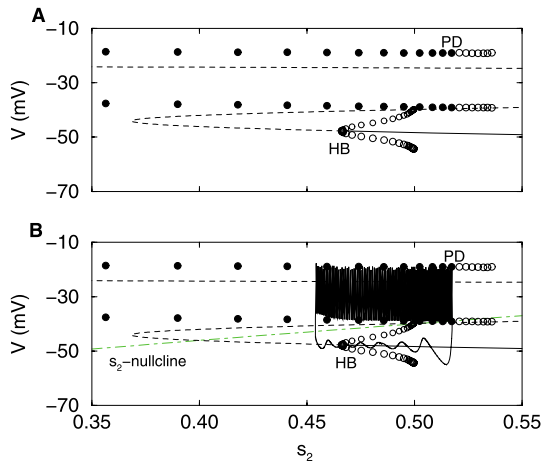


Fig. 4 (A) Bifurcation diagram of the V - n - s_1 fast subsystem, with s_2 as the bifurcation parameter ($g_{K1} = 20$ pS). The branch of closed circles represents stable spiking solutions, while open circles represent unstable spiking or subthreshold oscillations. HB=subcritical Hopf bifurcation, PD=period doubling bifurcation. (B) Fast subsystem bifurcation diagram with the s_2 -nullcline (green, dot-dashed curve) and the burst trajectory superimposed. (Color figure online.)

tion, at which point a branch of stable period-doubled oscillations is born. However, the trajectory does not follow this new branch, but instead winds in toward the lower stationary branch, which is only weakly attracting in the vicinity of the subcritical HB. This slow winding is reflected in subthreshold oscillations in the fast variables (V , n , s_1). The silent phase ends after the trajectory moves past the subcritical HB.

5. Episodic bursting

In the previous two examples of bursting, one or the other of the two slow variables was primarily responsible for driving the oscillation. We now show an example where the two slow variables contribute to the system dynamics in unique ways to produce episodic or compound bursting. In Fig. 5, the I_{K1} conductance is increased to $g_{K1} = 22$ pS, producing a series of fast bursts. Each burst episode is followed by a very long silent phase, or “desert,” after which another burst episode is produced (Fig. 5A). Small subthreshold oscillations are produced immediately prior to and immediately after each episode, but are not present during an episode. The period of a compound burst, approximately 110 s, is much longer than that of the bursting oscillations in earlier figures, largely due to the long desert.

The s_1 time course (Fig. 5B) reflects the V time course. During the active phase of each fast burst within an episode, s_1 rises and is primarily responsible for terminating the active phase. The decline of s_1 during the subsequent silent phase ultimately leads to the initiation of a new fast burst. Thus, the s_1 time course during a burst episode is very similar to that in Fig. 2, where s_1 is primarily responsible for driving the bursting. As in Fig. 2, small increases and decreases in s_2 occur during and after each fast burst. Moreover, the

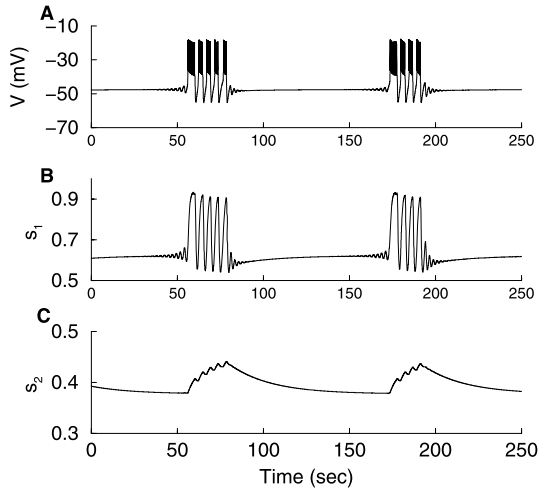


Fig. 5 (A) Episodic bursting obtained with $g_{K1} = 22$ pS. (B) Activity-dependent oscillations in s_1 drive the fast bursts within a burst episode. (C) Activity-dependent oscillations in s_2 initiate the burst episodes and the deserts.

mean value of s_2 accumulates during a burst episode (Fig. 5C), and when it becomes sufficiently large the burst episode itself is terminated. During the subsequent desert s_2 slowly declines, and it is this that determines the desert duration. Thus, the dynamics of s_1 are responsible for the fast bursts, while the dynamics of s_2 are responsible for the burst episodes.

The episodic bursting oscillation is best examined in the $V-s_2$ plane, treating s_2 as the sole slow variable, as in Fig. 4. To focus in on the interesting part of the diagram, only the interval $[0.35, 0.45]$ is shown in Fig. 6. As in Fig. 4, the bottom branch of the z -curve loses stability at a subcritical Hopf bifurcation. Also as in Fig. 4, the spiking branch loses stability before the homoclinic bifurcation is reached. This occurs through a sequence of period doublings, giving rise to a new stable branch of fast bursting oscillations. This transition, from spiking to bursting through a sequence of period doublings, has been analyzed in detail with bursting models containing a single slow variable (Chay and Rinzel, 1985; Terman, 1992). In these studies, the applied current was varied to obtain the transition sequence. The fast bursting oscillations in the current model are driven entirely by s_1 ; they persist when s_2 is clamped at an appropriate value (i.e., between 0.40 and 0.43) and can be analyzed using a fast/slow analysis with s_1 as the single slow variable. In the diagram, the minimum and maximum voltage of the spikes in the fast burst are represented by blue squares.

The s_2 nullcline and the compound bursting trajectory of the full system are superimposed on the bifurcation diagram in Fig. 6. The trajectory has been color coded so that bursts are shown alternately as red or black. During the first burst of an episode (leftmost red burst) the trajectory moves rightward along the spiking branch until the branch loses stability. However, rather than returning to the stable stationary branch, the trajectory follows the stable fast bursting branch and begins a sequence of bursts. That is, beyond the period doublings (PD), a hyperpolarized steady state and a bursting limit cycle coexist and

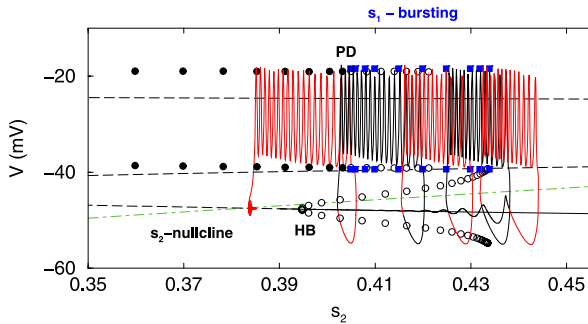


Fig. 6 Fast/slow analysis of episodic bursting ($g_{K1} = 22$ pS), with s_2 treated as the sole slow variable. There is now a branch of fast bursting oscillations (blue squares) that comes about following a sequence of period doubling (PD) bifurcations. (Color figure online.)

are both stable. The trajectory is attracted to the limit cycle, rather than the steady state, because it begins in the basin of attraction of the limit cycle. As the trajectory moves along the fast bursting branch it travels rightward since the mean voltage lies above the s_2 nullcline. The fast bursting branch terminates when it comes into contact with the branch of saddle points, and the trajectory (rightmost red burst) leaves the branch and is attracted to the stable stationary branch.

Because the stable steady states are near a Hopf bifurcation, they are only weakly attracting and have complex eigenvalues. For this reason, the trajectory oscillates noticeably as it approaches the stationary branch. These oscillations dampen out as the trajectory moves very slowly leftward. When g_{K1} was increased from 20 pS to 22 pS, the subcritical Hopf bifurcation (HB) migrated leftward, closer to the s_2 nullcline. For this reason, the motion along the stationary branch is considerably slower for this case than for the case of slow bursting ($g_{K1} = 20$ pS, Fig. 4). It is this slow motion that produces the desert between burst episodes (Fig. 5A). Once the trajectory moves past the subcritical HB, it remains close to the now unstable stationary branch. This slow passage through a subcritical HB has been analyzed previously (Baer et al., 1989). Eventually the trajectory spirals away from the stationary branch, producing small-amplitude oscillations (the unstable steady states have complex eigenvalues with positive real part). When it returns to the stable spiking branch a new episode of bursts begins.

6. Noise disrupts the fine structure, but episodic bursting persists

How sensitive to noise is episodic bursting produced through this mechanism? To investigate this question, we performed stochastic simulations, adding random noise to the conductance of the voltage-independent leak current (see mathematical model section). Figure 7 shows simulations with various values of N_{stoc} , the number of stochastic leakage channels. Small values of N_{stoc} correspond to large values of the noise intensity parameter σ . When $N_{stoc} = 1100$, the noise is small, so the V time course (Fig. 7A) is similar to the deterministic time course. When the channel number is reduced to $N_{stoc} = 200$ there is little change in the episodic bursting (Fig. 7B). However, the small subthreshold oscillations that are normally visible before and after each burst episode are now obscured by

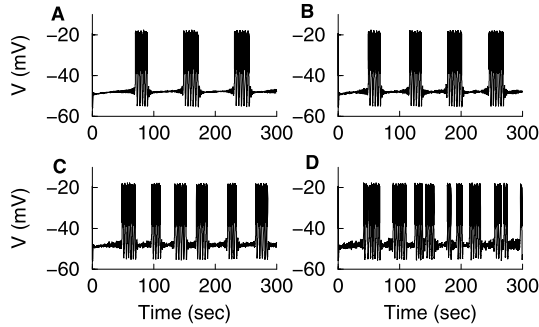


Fig. 7 Episodic bursting persists, but some of the fine structure is lost in the presence of channel noise. (A) $N_{stoc} = 1100$, (B) $N_{stoc} = 200$, (C) $N_{stoc} = 35$, (D) $N_{stoc} = 15$. In each case, $g_{leak} = 41$ pS.

the noise. Also, the episode period is now shorter. When $N_{stoc} = 35$, some of the deserts end prematurely (Fig. 7C). In this case, the noise pushes the phase point out of the small basin of attraction of the steady states on the bottom branch of the z -curve (see Fig. 7), into the basin of the fast bursting solutions. The desert is particularly sensitive to noise, since the phase point moves very slowly along the bottom branch during a desert and the basin of attraction shrinks to zero as the subcritical Hopf bifurcation is approached. With channel number $N_{stoc} = 15$, the long deserts have disappeared, but bursting is still episodic (Fig. 7D). This demonstrates that some of the fine structure of episodic bursting produced through this mechanism (i.e., subthreshold oscillations and long deserts) is lost in the presence of noise, but the episodic bursting itself persists.

We have performed longer simulations (3,000 seconds of simulation time) and calculated, for each simulation, the mean desert duration, mean episode duration, and mean burst duration within an episode. When comparing the low-noise case ($N_{stoc} = 1100$) to the high-noise case ($N_{stoc} = 15$), we found that the mean burst duration decreased by 22%, the mean episode duration decreased by 27%, and the mean desert duration decreased by 67%. It is, therefore, clear that the desert duration is most affected by random channel noise.

7. Episodic bursting is moderately robust to changes in parameter values

Another measure of robustness of a system is how sensitive it is to variation of parameters. In our model, the two key physiological parameters are the maximal conductances g_{K1} and g_{K2} of the two slow K^+ currents, I_{K1} and I_{K2} . We, therefore, vary these two parameters over a square region in parameter space centered at $g_{K1} = 22$ pS, $g_{K2} = 16$ pS (parameter values used in Figs. 5, 6, and 7). We superimpose a lattice on this region and sample the behavior of the system (without noise) at each lattice point. Figure 8 shows the distribution of behaviors on this lattice. When g_{K1} and g_{K2} are both large, the system comes to rest (black region), since the K_1 and K_2 currents are both hyperpolarizing and thus suppress the electrical activity. When both conductances are small, the system spikes continuously (blue region), since now the amount of hyperpolarizing current is too small to terminate a burst. All the bursting behaviors exist in a diagonal band between continuous spiking and the silent state. Fast bursting (green region) occurs when g_{K1} is at an

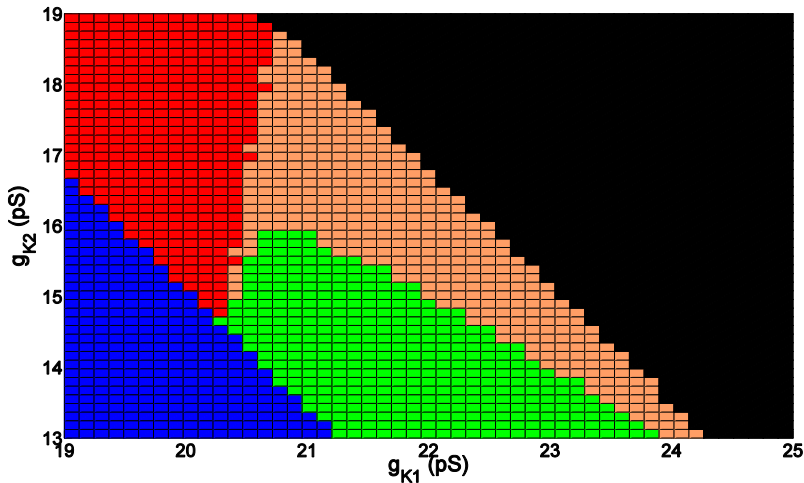


Fig. 8 Distribution of model behaviors on a square lattice centered at $g_{K1} = 22$ pS, $g_{K2} = 16$ pS. Color coding is as follows: (black) silent, (red) slow bursting, (green) fast bursting, (tan) episodic bursting, (blue) constant spiking. Episodic bursting occurs over a moderately large region of the lattice, but other behaviors extend outside the range of the lattice. (Color figure online.)

intermediate value and g_{K2} is small, since in this case, the K_1 current is sufficiently large to terminate the bursts, but not so large that it suppresses all activity. Slow bursting (red region) occurs when g_{K1} is so small that the K_1 current is unable to terminate the burst and significant variation in s_2 is required. Finally, episodic bursting (tan region) occurs at intermediate values of g_{K1} and g_{K2} . Although not as large as the other regions (which continue out beyond the range of the lattice), there is a sizeable region of the lattice for which episodic bursting occurs. However, the period of the episodic bursting is very sensitive to changes in the conductances. For example, if $g_{K2} = 16$ pS and g_{K1} is varied from 21.8 pS to 22.4 pS, the period goes from 85 sec to 310 sec. Therefore, episodic bursting is moderately robust to g_{K1} , g_{K2} parameter variation, but the period is very sensitive to changes in the parameter values.

8. Discussion

We have previously shown that a model of bursting with two slow variables, s_1 and s_2 , with disparate time scales is capable of producing three types of bursting: fast bursting driven by s_1 , slow bursting driven by s_2 , and medium bursting with an intermediate period driven by both s_1 and s_2 (Bertram et al., 2000). The bursting driven by both slow variables was termed “phantom bursting,” and the model described as a “phantom bursting model.” In the current article, we have demonstrated that the phantom bursting model can produce a fourth type of bursting behavior, episodic bursting. This uses the same phantom bursting model that was used in the previous study, but in a different region of parameter space, where the two slow variables interact so that s_1 drives the fast bursts within an episode and s_2 clusters the fast bursts into episodes followed by deserts.

The episodic bursting produced with the phantom bursting model is characterized by subthreshold oscillations immediately prior to and after each burst episode. However, in the presence of even a small amount of noise, these small oscillations are no longer discernable. This is potentially important, since in the two cell types that we are aware of that produce episodic bursting, pancreatic β -cells within intact islets of Langerhans and GnRH-secreting neurons of the hypothalamus, no patterned subthreshold oscillations are observed. However, in each case the noise endogenous to the cells is sufficient to obscure any patterned subthreshold oscillations. Thus, the mechanism for episodic bursting that we describe here could potentially apply to either of these systems.

While this mechanism for episodic bursting could describe the behavior of pancreatic β -cells, another mechanism is possible. Glucose metabolism plays a key signaling role in these cells, and there is considerable evidence for metabolic oscillations (Bertram et al., 2007; Tornheim, 1997). We have proposed that these oscillations are responsible for clustering fast bursts into episodes in the β -cells (Bertram et al., 2004). One way to distinguish between the two mechanisms is through the use of random channel noise. We showed in Fig. 7 that channel noise has its greatest effect on the desert duration between burst episodes. That is, the mean desert duration decreases much more rapidly than does the episode duration or burst duration as the intensity of the noise is increased. This is in contrast to episodic bursting driven by metabolic oscillations. In this Dual Oscillator Model (DOM), channel noise has little effect on the desert duration and the duration of an episode, but greatly reduces the duration of individual bursts within an episode (Pedersen, 2007). The desert and episode durations are little effected by noise because these two features are determined by oscillations in glycolysis, which are largely independent of the cell's electrical activity. Thus, channel noise has little impact on the glycolytic oscillator that clusters the bursts together into episodes. However, the bursts that occur within an episode are driven by electrical events, and are susceptible to perturbation from channel noise. In particular, the individual bursts are produced through a phantom bursting mechanism involving the Ca^{2+} concentration in the cytosol (the s_1 variable) and the endoplasmic reticulum (the s_2 variable) acting through a Ca^{2+} activated K^+ channel (Bertram and Sherman, 2004). As shown in Pedersen (2007), phantom bursting is quite sensitive to noise, more so than the typical bursting driven by a single slow variable. Thus, in both the DOM and the phantom bursting model for episodic bursting, it is the phantom bursting component (the component involving slow changes in the s_2 variable) that is most sensitive to noise.

Pancreatic β -cells are coupled together by gap junctions to form islets. In this physiological state, the channel noise in the important ATP-sensitive K^+ channels is shared by all the cells in the islet, reducing its impact (Atwater et al., 1983; Chay and Kang, 1988; Sherman et al., 1988). However, when isolated β -cells are examined, they tend to be much noisier (Kinard et al., 1999). Thus, if an islet produces episodic bursting, as is often the case, then the phantom model for episodic bursting suggests that isolated β -cells would typically produce fast bursting, with some clustering (like Fig. 7D). However, as was shown by Pedersen (2007), the DOM suggests that isolated β -cells would typically produce slow bursting. Interestingly, β -cells typically exhibit either fast or slow bursting when isolated from the islet, which is consistent with both models.

The model that we have used is minimal, with two fast and two slow variables. In this model, the slow variables represent activation variables of hyperpolarizing K^+ currents. However, similar behaviors could be achieved by defining the slow variables in other

ways, such as inactivation variables of depolarizing currents, or as a combination of activation and deactivation. That is, the behaviors that we describe are not restricted to the specific details of the model. In addition, more complex neuron or endocrine cell models could in principle also achieve the behaviors produced by this minimal model, as long as the model possesses at least two slow variables with disparate time scales.

Acknowledgements

The authors thank Arthur Sherman and Charles Zimlik for early discussions of the phantom mechanism for compound bursting. This work was partially supported by NSF grant DMS-0613179 to R.B., and was begun while W.P.C. was a student at an NSF-sponsored REU program in mathematical biology at Penn State Erie.

References

- Alving, B.O., 1986. Spontaneous activity in isolated somata of *Aplysia* pacemaker neurons. *J. Gen. Physiol.* 51, 29–45.
- Atwater, I., Rosario, L., Rojas, E., 1983. Properties of the Ca-activated K^+ channel in pancreatic β -cells. *Cell Calcium* 4, 451–461.
- Baer, S.M., Erneux, T., Rinzel, J., 1989. The slow passage through a Hopf bifurcation: delay, memory effects, and resonance. *SIAM J. Appl. Math.* 49, 55–71.
- Bertram, R., Sherman, A., 2004. A calcium-based phantom bursting model for pancreatic islets. *Bull. Math. Biol.* 66, 1313–1344.
- Bertram, R., Butte, M., Kiemel, T., Sherman, A., 1995. Topological and phenomenological classification of bursting oscillations. *Bull. Math. Biol.* 57, 413–439.
- Bertram, R., Previte, J., Sherman, A., Kinard, T.A., Satin, L.S., 2000. The phantom burster model for pancreatic β -cells. *Biophys. J.* 79, 2880–2892.
- Bertram, R., Satin, L., Zhang, M., Smolen, P., Sherman, A., 2004. Calcium and glycolysis mediate multiple bursting modes in pancreatic islets. *Biophys. J.* 87, 3074–3087.
- Bertram, R., Sherman, A., Satin, L.S., 2007. Metabolic and electrical oscillations: partners in controlling pulsatile insulin secretion. *Am. J. Physiol.* 293, E890–E900.
- Chay, T.R., Kang, H.S., 1988. Role of single-channel stochastic noise on bursting clusters of pancreatic β -cells. *Biophys. J.* 54, 427–435.
- Chay, T.R., Keizer, J., 1983. Minimal model for membrane oscillations in the pancreatic β -cell. *Biophys. J.* 42, 181–190.
- Chay, T.R., Rinzel, J., 1985. Bursting, beating, and chaos in an excitable membrane model. *Biophys. J.* 47, 357–366.
- Coombes, S., Bressloff, P.C. (Eds.), 2005. *Bursting: The Genesis of Rhythm in the Nervous System*. World Scientific, Singapore.
- Crunelli, V., Kelly, J.S., Leresche, N., Pirchio, M., 1987. The ventral and dorsal lateral geniculate nucleus of the rat: intracellular recordings in vitro. *J. Physiol. (Lond.)* 384, 587–601.
- de Vries, G., Sherman, A., 2000. Channel sharing in pancreatic β -cells revisited: enhancement of emergent bursting by noise. *J. Theor. Biol.* 207, 513–530.
- Dean, P.M., Mathews, E.K., 1970. Glucose-induced electrical activity in pancreatic islet cells. *J. Physiol.* 210, 255–264.
- Del Negro, C.A., Hsiao, C.-F., Chandler, S.H., Garfinkel, A., 1998. Evidence for a novel bursting mechanism in rodent trigeminal neurons. *Biophys. J.* 75, 174–182.
- Ermentrout, G.B., 2002. *Simulating, Analyzing, and Animating Dynamical Systems: A Guide to XPPAUT for Researchers and Students*. SIAM, Philadelphia.
- Fox, R.F., 1997. Stochastic versions of the Hodgkin–Huxley equations. *Biophys. J.* 72, 2068–2074.
- Henquin, J.C., Meissner, H.P., Schmeer, W., 1982. Cyclic variations of glucose-induced electrical activity in pancreatic B cells. *Pflügers Arch.* 393, 322–327.

- Kinard, T.A., Vries, G., Sherman, A., Satin, L.S., 1999. Modulation of the bursting properties of single mouse pancreatic β -cells by artificial conductances. *Biophys. J.* 76, 1423–1435.
- Kuehl-Kovarik, M.C., Pouliot, W.A., Halterman, G.L., Handa, R.J., Dubek, F.E., Partin, K.M., 2002. Episodic bursting activity and response to excitatory amino acids in acutely dissociated gonadotropin-releasing hormone neurons genetically targeted with green fluorescent protein. *J. Neurosci.* 22, 2313–2322.
- Pedersen, M.G., 2007. Phantom bursting is highly sensitive to noise and unlikely to account for slow bursting in β -cells: considerations in favor of metabolically driven oscillations. *J. Theor. Biol.* 248, 391–400.
- Rinzel, J., 1985. Bursting oscillations in an excitable membrane model. In: Sleeman, B.D., Jarvis, R.J. (Eds.), *Ordinary and Partial Differential Equations, Lecture Notes in Mathematics*, pp. 304–316. Springer, New York.
- Rinzel, J., 1987. A formal classification of bursting mechanisms in excitable systems. In: Teramoto, E., Yamaguti, M. (Eds.), *Mathematical Topics in Population Biology, Morphogenesis and Neurosciences*. Springer, Berlin.
- Rinzel, J., Ermentrout, G.B., 1998. Analysis of neural excitability and oscillations. In: Koch, C., Segev, I. (Eds.), *Methods in Neuronal Modeling: From Ions to Networks*, pp. 251–291. MIT Press, Cambridge.
- Sherman, A., Rinzel, J., Keizer, J., 1988. Emergence of organized bursting in clusters of pancreatic β -cells by channel sharing. *Biophys. J.* 54, 411–425.
- Smolen, P., Terman, D., Rinzel, J., 1993. Properties of a bursting model with two slow inhibitory variables. *SIAM J. Appl. Math.* 53, 861–892.
- Stojilkovic, S.S., Kukuljan, M., Iida, T., Rojas, E., Catt, K.J., 1992. Integration of cytoplasmic calcium and membrane potential oscillations maintains calcium signaling in pituitary gonadotrophs. *Proc. Natl. Acad. Sci.* 89, 4081–4085.
- Suter, K.J., Wuarin, J.-P., Smith, B.N., Dudek, F.E., Moenter, S.M., 2000. Whole-cell recordings from preoptic/hypothalamic slices reveal burst firing in gonadotropin-releasing hormone neurons identified with green fluorescent protein in transgenic mice. *Endocrinology* 141, 3731–3736.
- Terman, D., 1992. The transition from bursting to continuous spiking in excitable membrane models. *J. Nonlinear Sci.* 2, 135–182.
- Tornheim, K., 1997. Are metabolic oscillations responsible for normal oscillatory insulin secretion? *Diabetes* 46, 1375–1380.
- Wong, R.K.S., Prince, D.A., 1981. Afterpotential generation in hippocampal pyramidal cells. *J. Neurophysiol.* 45, 86–97.
- Zhang, M., Goforth, P., Sherman, A., Bertram, R., Satin, L., 2003. The Ca^{2+} dynamics of isolated mouse β -cells and islets: implications for mathematical models. *Biophys. J.* 84, 2852–2870.